PNAS RESEARCH ARTICLE | IMMUNOLOGY AND INFLAMMATION

Dual modifying of MAVS at lysine 7 by SIRT3-catalyzed deacetylation and SIRT5-catalyzed desuccinylation orchestrates antiviral innate immunity

Xing Liu[a,b,c,d,e,1], Chunchun Zhu[a,b,c,d,1], Shuke Jia[a,c], Hongyan Deng[a], Jinhua Tang[a,c], Xueyi Sun[a,c], Xiaoli Zeng[a,c], Xiaoyun Chen[a,c], Zixuan Wang[a,c], Wen Liu[a,c], Qian Liao[a,c], Huangyuan Zha[a], Xiaolian Cai[a,c], and Wuhan Xiao[a,b,c,d,e,2]

Edited by Michael S. Diamond, Washington University in St. Louis School of Medicine, St. Louis, MO; received August 17, 2023; accepted March 20, 2024 by Editorial Board Member Katherine A. Fitzgerald

To effectively protect the host from viral infection while avoiding excessive immunopathology, the innate immune response must be tightly controlled. However, the precise regulation of antiviral innate immunity and the underlying mechanisms remain unclear. Here, we find that sirtuin3 (SIRT3) interacts with mitochondrial antiviral signaling protein (MAVS) to catalyze MAVS deacetylation at lysine residue 7 (K7), which promotes MAVS aggregation, as well as TANK-binding kinase I and IRF3 phosphorylation, resulting in increased MAVS activation and enhanced type I interferon signaling. Consistent with these findings, loss of *Sirt3* in mice and zebrafish renders them more susceptible to viral infection compared to their wild-type (WT) siblings. However, *Sirt3* and *Sirt5* double-deficient mice exhibit the same viral susceptibility as their WT littermates, suggesting that loss of *Sirt5* in *Sirt3*-deficient mice may counteract the increased viral susceptibility displayed in *Sirt3*-deficient mice. Thus, we not only demonstrate that SIRT3 positively regulates antiviral immunity in vitro and in vivo, likely via MAVS, but also uncover a previously unrecognized mechanism by which SIRT3 acts as an accelerator and SIRT5 as a brake to orchestrate antiviral innate immunity.

SIRT3 | SIRT5 | MAVS | deacetylation | desuccinylation

Significance

As the first line of defense against viral infection, innate immunity must be precisely controlled. Mitochondrial antiviral signaling protein (MAVS) is a critical adaptor protein in the retinoic-acid inducible gene I (RIG-I)-like receptor (RLR) signaling pathway. In this study, we found that sirtuin3 (SIRT3) interacts with MAVS to catalyze MAVS deacetylation at lysine residue 7 (K7), thereby promoting MAVS activation, in contrast to SIRT5-mediated MAVS desuccinylation at K7. Loss of *Sirt3* renders the host more susceptible to viral infection compared to its wild-type siblings. However, *Sirt3* and *Sirt5* double-deficient mice exhibit the same viral susceptibility as their wild-type littermates. Our results suggest that SIRT3 serves as an accelerator and SIRT5 as a brake to orchestrate antiviral innate immunity.

The mitochondrial antiviral signaling protein (MAVS) (also known as IPS1, VISA, or Cardif) serves as a key hub in innate immunity against RNA viruses, localizes to the mitochondrial outer membrane (1–4). Upon RNA virus infection, MAVS forms prion-like aggregates by receiving the cytosolic retinoic acid-inducible gene I (RIG-I)-activated signal and subsequently forms a complex with TANK-binding kinase I (TBK1)/Iκ-B kinase ε (IKK-ε), leading to activation of the type I interferon signaling (2, 3, 5–7). In the resting states, MAVS is prevented from spontaneous aggregation to turn off the type I interferon signaling and maintain immune homeostasis (8).

Due to the importance of posttranslational modifications (PTMs) in regulating the activity, stability, and folding of target proteins by inducing their covalent attachment to new functional groups, PTMs on MAVS may play a pivotal role in the regulation of antiviral innate immune signaling (6, 9–22). Recently, we identified that SIRT5 desuccinylates MAVS at K7 to reduce MAVS aggregation, but its succinyltransferase is still unclear (22).

Sirtuin 3 (SIRT3) belongs to a conserved family of NAD^+-dependent protein deacetylases involved in metabolism, stress response, and longevity (23). Among the seven mammalian sirtuins (SIRT1-7), SIRT3 is mainly localized to the mitochondria and serves as one of the most prominent deacetylases that can regulate acetylation levels in mitochondria, leading to the activation of many oxidative pathways (24–26). Some evidence suggests that the deacetylase activity of SIRT3 is associated with inflammation and suppression of virus production (27, 28), but whether *SIRT3* is involved in antiviral innate immunity is poorly understood.

Here, we show that SIRT3 positively regulates antiviral innate immune responses both in vitro and in vivo, likely via MAVS.

Results

SIRT3 Positively Regulates the MAVS-Mediated Antiviral Innate Immune Response. Upon infection with Sendai virus (SeV) in H1299 cells, overexpression of *SIRT3* (Flag-*SIRT3*) caused a significant increase in *IFNβ*, *CXCL10,* and *ISG15* mRNA compared to transfection of the empty vector control (Flag empty) (Fig. 1 *A*–*C*). In contrast, disruption of *SIRT3* in H1299 cells resulted in a reduction of *IFNβ*, *CXCL10,* and *ISG15* mRNA

Author contributions: X.L., C.Z., and W.X. designed research; X.L., C.Z., S.J., H.D., and J.T. performed research; S.J., H.D., J.T., X.S., X. Chen, Z.W., W.L., Q.L., H.Z., and X. Cai contributed new reagents/analytic tools; X.L., C.Z., X.Z., and W.X. analyzed data; and X.L., C.Z., and W.X. wrote the paper.

The authors declare no competing interest.

This article is a PNAS Direct Submission. M.S.D. is a guest editor invited by the Editorial Board.

[1]X.L. and C.Z. contributed equally to this work.

[2]To whom correspondence may be addressed. Email: w-xiao@ihb.ac.cn.

This article contains supporting information online at https://www.pnas.org/lookup/suppl/doi:10.1073/pnas.2314201121/-/DCSupplemental.

Published April 18, 2024.

in response to SeV infection (Fig. 1 *D*–*F*). Furthermore, SeV-induced IRF3 phosphorylation was reduced in *SIRT3*-deficient H1299 cells (*SIRT3*$^{-/-}$) compared to wild-type (WT) H1299 cells (*SIRT3*$^{+/+}$) (Fig. 1 *G* and *H*). Consistent with these findings, SeV propagation was increased in *SIRT3*$^{-/-}$ H1299 cells compared to that in *SIRT3*$^{+/+}$ H1299 cells as shown by immunoblotting for SeV protein (Fig. 1 *G* and *H*). VSV (Vesicular Stomatitis Virus)-GFP virus proliferation was increased in *SIRT3*$^{-/-}$ H1299 cells compared to that in *SIRT3*$^{+/+}$ H1299 cells as revealed by fluorescence microscopy imaging and immunoblotting (Fig. 1*I*). Similar results were obtained in HEK293T cells or H1299 cells (*SI Appendix*, Fig. S1 *A*–*F*). These data suggest that *SIRT3* positively regulates type I interferon signaling during RNA virus infection.

The viral RNA analog poly (I:C) LMW (low molecular weight) and HMW (high molecular weight) are the ligands for RIG-I and MDA5, respectively (Fig. 1*J*) (29). To determine which molecule is targeted by SIRT3, we used poly (I:C) LMW and HMW to activate RLR signaling respectively and then examined the effect of *SIRT3* in this pathway. Overexpression of *SIRT3* caused an increase of *IFNβ* mRNA upon both poly (I:C) LMW and HMW stimulation in H1299 cells (Fig. 1*K*), but disruption of *SIRT3* in H1299 cells caused a reduction of *IFNβ* mRNA compared to that in WT H1299 cells (*SIRT3*$^{+/+}$) upon both poly (I:C) LMW and HMW stimulation (Fig. 1*L*). These data suggest that SIRT3 may target the merged molecule of the RIG-I pathway and MDA5 pathways, MAVS (Fig. 1*J*).

Overexpression of *SIRT3* enhanced the luciferase activity of IFNβ promoter reporter (IFNβ-luc) and ISRE reporter (ISRE-luc) induced by ectopic expression of *MAVS* (Fig. 1 *M* and *N*). Consistent with these findings, overexpression of *SIRT3* also promoted *IFNβ* mRNA expression induced by ectopic expression of *MAVS* (Fig. 1*O*). Furthermore, compared with those in *Mavs*-intact (*Mavs*$^{+/+}$) mouse embryonic fibroblast cells (MEF), overexpression of *Sirt3* in *Mavs*-deficient MEF cells had no apparent effect on the induction of *Ifnβ, Isg15*, *Cxcl10,* and *Ifit1* mRNA upon VSV infection (Fig. 1 *P*–*S*). Consistent with these observations, *Sirt3* overexpression attenuated VSV-GFP virus propagation in *Mavs*$^{+/+}$ MEF cells, but *Sirt3* overexpression had no apparent effect on VSV-GFP virus propagation in *Mavs*$^{-/-}$ MEF cells, as shown by fluorescence microscopy imaging and immunoblotting (Fig. 1 *T* and *U*).

To exclude the possibility that these phenomena were due to a direct effect of Sirt3 on VSV replication, we further used the viral RNA analog poly (I:C) LMW and HMW to repeat these assays. As shown in Fig. 1 *V*–*X*, in *Mavs*$^{+/+}$ MEF cells, *Sirt3* overexpression caused an increase of *Ifnβ*, *Isg15*, and *Cxcl10* mRNA induced by the transfection with poly (I:C) LMW or HMW, whereas in *Mavs*$^{-/-}$ MEF cells, *Sirt3* overexpression had no apparent effect on the induction of *Ifnβ*, *Isg15*, and *Cxcl10* mRNA.

Taken together, these data suggest that *SIRT3* positively regulates RLR signaling by targeting MAVS.

SIRT3 Interacts with MAVS to Enhance MAVS Function Depending on Its Enzymatic Activity. Notably, neither *SIRT3* overexpression nor *SIRT3* deletion affected MAVS protein levels (*SI Appendix*, Fig. S2 *A* and *B*). Furthermore, *SIRT3* expression was not affected by VSV infection (*SI Appendix*, Fig. S2*C*).

The coimmunoprecipitation (Co-IP) assay showed that ectopically expressed MAVS interacted with ectopically expressed SIRT3 (Fig. 2 *A* and *B*), and endogenous MAVS and SIRT3 could also be coimmunoprecipitated (Fig. 2*C*). As expected, overexpressed SIRT3 was localized to mitochondria, and VSV infection promoted the colocalization of SIRT3 with TOM20, an outer mitochondrial membrane protein (*SI Appendix*, Fig. S3*A*). SIRT3 colocalized with MAVS and VSV infection enhanced their colocalization (Fig. 2*D*). The interaction between SIRT3 and MAVS was further confirmed by PLA (Fig. 2*E*). Due to the lack of a suitable anti-SIRT3 antibody that can detect endogenous SIRT3 by immunofluorescence staining (*SI Appendix*, Fig. S3 *B*–*D*), in order to mimic endogenous SIRT3 and obtain information about endogenous SIRT3 localization, we overexpressed *SIRT3* at a relatively low dose in *SIRT3*$^{-/-}$ H1299 cells to achieve comparable endogenous levels of SIRT3 in H1299 cells (*SI Appendix*, Fig. S3*E*) and then examined the colocalization between SIRT3 and MAVS. Similar to the above observations (*SI Appendix*, Fig. S3*A* and Fig. 2*D*), upon VSV infection, SIRT3 colocalized with TOM20 and MAVS (*SI Appendix*, Fig. S3 *F* and *G*). Domain mapping revealed that the TM domain of MAVS was required for SIRT3 binding (*SI Appendix*, Fig. S4 *A*–*C*).

In A549 cells, overexpression of WT SIRT3 enhanced VSV-induced expression of *IFNβ* and *CXCL10*, but ectopic expression of SIRT3-H248Y, an enzymatically inactive SIRT3 mutant (30), did not enhance VSV-induced expression of *IFNβ* and *CXCL10* (Fig. 2 *F* and *G*). Consistent with these findings, overexpression of WT SIRT3 significantly suppressed VSV-GFP virus propagation, but ectopic expression of SIRT3-H248Y did not (Fig. 2 *H*–*J*). Similarly, reconstitution of WT SIRT3 enhanced VSV- or SeV-induced expression of *IFNβ* and *CXCL10*, but reconstitution of SIRT3-H248Y did not enhance VSV- or SeV-induced expression of *IFNβ* and *CXCL10* (Fig. 2 *K* and *L* and *SI Appendix*, Fig. S4 *D* and *E*).

To further validate that the effect of *SIRT3* on RLR signaling is dependent on its enzymatic activity, we took advantage of its specific inhibitor, 3-TYP (31). First, we confirmed that 3-TYP did not affect cell apoptosis and viability when used in the range of 10 to 200 μM (*SI Appendix*, Fig. S5 *A* and *B*). Treatment with 3-TYP suppressed the expression of *IFNβ* and *CXCL10* in VSV-infected THP-1 cells (*SI Appendix*, Fig. S5 *C* and *D*). Similarly, 3-TYP treatment also suppressed the expression of *IFNβ*, *CXCL10,* and *ISG15* in VSV-infected A549 cells (*SI Appendix*, Fig. S5 *E*–*G*). To exclude a direct effect of 3-TYP on viral replication, we repeated these assays using the viral RNA analog poly (I:C) LMW. Treatment with 3-TYP suppressed the expression of *IFNβ* and *CXCL10* in poly (I:C) LMW-transfected H1299 cells (*SI Appendix*, Fig. S5 *H* and *I*). In *SIRT3*$^{-/-}$ H1299 cells, treatment with 3-TYP had no apparent effect on the expression of *IFNβ* and *CXCL10* in poly (I:C) LMW-transfected H1299 cells (*SI Appendix*, Fig. S5 *H* and *I*).

Taken together, these data suggest that SIRT3 binds to MAVS and inhibits MAVS activation in a manner dependent on its enzymatic activity.

SIRT3 Deacetylates MAVS at Lysine 7. In HEK293T cells, addition of the histone deacetylase inhibitors trichostatin A (TSA) and nicotinamide (NAM) caused a time-dependent increase in acetylation of overexpressed Flag-MAVS, as revealed by anti-pan-acetyl-K antibody after IP with anti-Flag antibody (*SI Appendix*, Fig. S6*A*). We further confirmed this result after using anti-pan-acetyl-K antibody for IP (Fig. 3*A*). Next, we used MEF cells to test whether endogenous Mavs is also acetylated. Addition of TSA and NAM caused acetylation of endogenous Mavs in *Mavs*$^{+/+}$ MEF cells, but not in *Mavs*$^{-/-}$ MEF cells (Fig. 3 *B* and *C*). Notably, acetylation of endogenous Mavs was higher in *Sirt3*$^{-/-}$ MEF cells than in *Sirt3*$^{+/+}$ MEF cells, suggesting that Sirt3 may target Mavs to catalyze MAVS deacetylation (Fig. 3*D*).

As shown in Fig. 3 *E* and *F*, overexpression of *SIRT3* had no enhancement effect on MAVS-K7R-induced expression of both *IFNβ* and *CXCL10* in HEK293T cells, but still caused an increase in other mutant-induced expression of both *IFNβ* and *CXCL10* in HEK293T cells. This lysine 7 is conserved not only between the mouse and human, but also between the human, macaque, cow, pig, dog, mouse, and rat (Fig. 3*G*). Thus, the conserved lysine

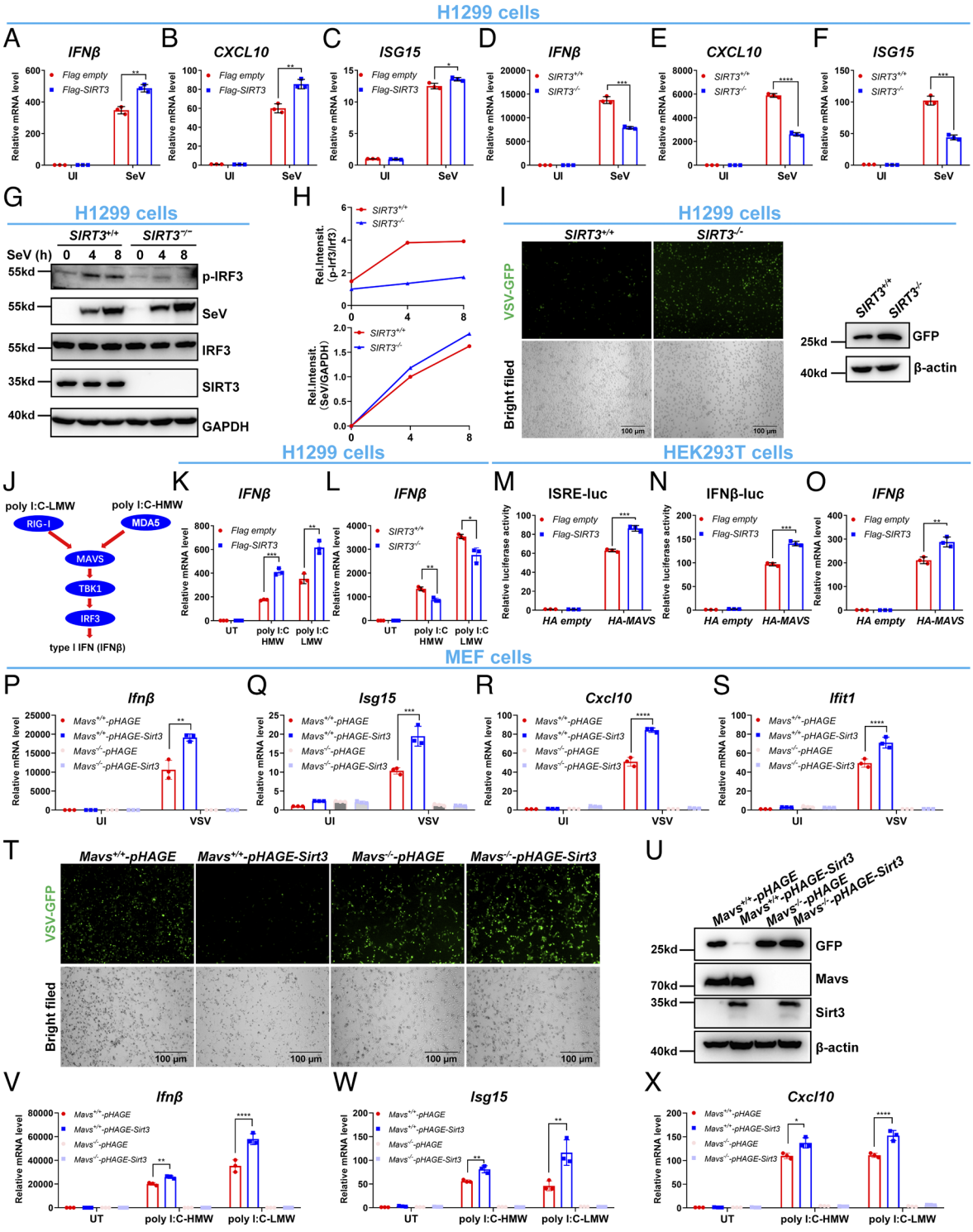

Fig. 1. SIRT3 activates the MAVS-mediated innate antiviral response. (*A*–*C*) qPCR analysis of *IFNβ* (*A*), *CXCL10* (*B*), and *ISG15* (*C*) mRNA in H1299 cells transfected with indicated plasmids for 24 h, and then left uninfected (UI) or infected with SeV for 8 h. (*D*–*F*) qPCR analysis of *IFNβ* (*D*), *CXCL10* (*E*), and *ISG15* (*F*) mRNA in *SIRT3*$^{-/-}$ or *SIRT3*$^{+/+}$ H1299 cells left UI or infected with SeV for 8 h. (*G*) Immunoblotting (IB) of whole cell lysates using the indicated antibodies in *SIRT3*$^{+/+}$ and *SIRT3*$^{-/-}$ H1299 cells UI or infected with SeV for 4 or 8 h. (*H*) Quantitation of phosphorylated IRF3 (p-IRF3) and SeV proteins shown in (*G*). (*I*) *SIRT3*$^{-/-}$ or *SIRT3*$^{+/+}$ H1299 cells were infected with VSV-GFP virus (MOI = 0.1) for 12 h, and viral infectivity was detected by fluorescence microscopy and immunoblotting. (*J*)Schematic of the working model of high molecular weight poly I:C (poly I:C-HMW) and low molecular weight poly I:C (poly I:C-LMW). (*K*) qPCR analysis of *IFNβ* mRNA in H1299 cells transfected with the indicated plasmids for 24 h, and then transfected without (UT) or with poly I:C HMW or poly I:C LMW for 8 h. (*L*) qPCR analysis of *IFNβ* mRNA in *SIRT3*$^{-/-}$ or *SIRT3*$^{+/+}$ H1299 cells transfected without (UT) or with high molecular weight poly I:C (poly I:C HMW) or low molecular weight poly I:C (poly I:C LMW) for 8 h. (*M*) ISRE reporter activity by cotransfection of HA-MAVS together with Flag empty vector (Flag empty) or with Flag-*SIRT3* in HEK293T cells for 24 h. (*N*) *IFNβ* promoter activity by cotransfection of HA-MAVS together with Flag empty vector (Flag empty) or with Flag-*SIRT3* in HEK293T cells for 24 h. (*O*) qPCR analysis of *IFNβ* mRNA upon cotransfection of HA-MAVS together with Flag empty vector (Flag empty) or with Flag-*SIRT3* in HEK293T cells for 24 h. (*P*–*S*) qPCR analysis of *Ifnβ* (*P*), *Isg15* (*Q*), *Cxcl10* (*R*), and *Ifit1* (*S*) mRNA in *Mavs*$^{+/+}$ and *Mavs*$^{-/-}$ MEF cells stably expressing empty vector or *Sirt3* (lentivirus infection), followed by infection without (UI) or with VSV for 8 h. (*T* and *U*) *Mavs*$^{+/+}$ and *Mavs*$^{-/-}$ MEF cells stably expressing empty vector or *Sirt3* were infected with VSV-GFP virus (MOI = 0.1) for 12 h, and viral infectivity was detected by fluorescence microscopy (*T*) and IB (*U*). (*V*–*X*) qPCR analysis of *Ifnβ* (*V*), *Isg15* (*W*), and *Cxcl10* (*X*) mRNA in *Mavs*$^{+/+}$ and *Mavs*$^{-/-}$ MEF cells stably expressing empty vector or *Sirt3*, followed by transfection without (UT) or with high molecular weight poly I:C (poly I:C HMW) or low molecular weight poly I:C (poly I:C LMW) for 8 h. **P* < 0.05, ***P* < 0.01, ****P* < 0.001, *****P* < 0.0001. Data from at least three independent experiments (mean ± SD) (*A*–*F*, *K*–*S*, and *V*–*X*].

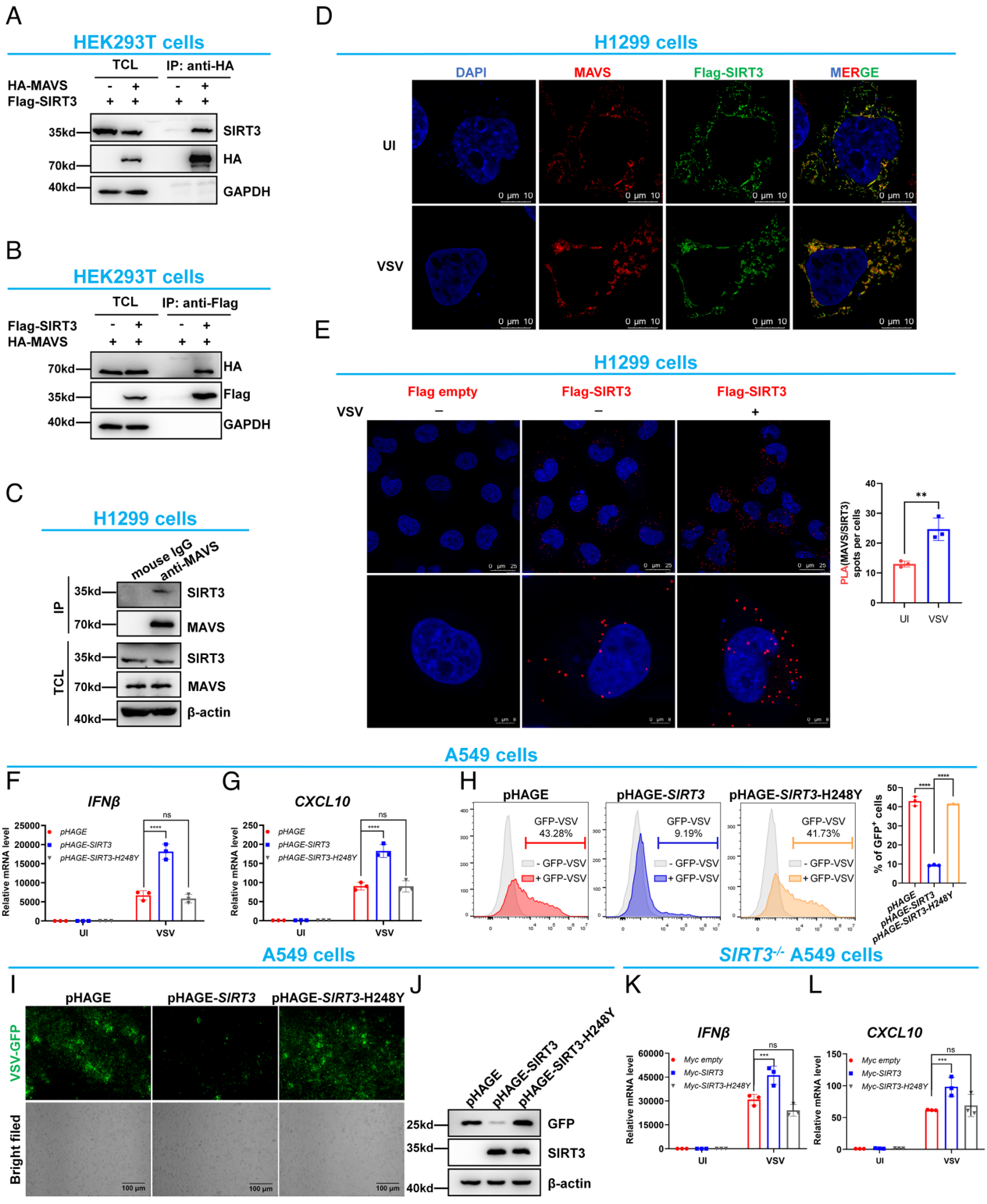

Fig. 2. SIRT3 interacts with MAVS to enhance MAVS activation depending on its enzymatic activity. (*A* and *B*) Co-IP of Flag-SIRT3 with HA-MAVS and vice versa. HEK293T cells were cotransfected with the indicated plasmids for 24 h. Anti-HA (*A*) or anti-Flag (*B*) antibody-conjugated agarose beads were used for IP, and the interaction was detected by immunoblotting with the indicated antibodies. (*C*) Endogenous interaction between MAVS and SIRT3. Anti-MAVS antibody was used for IP, and normal mouse IgG was used as a control. (*D*) Colocalization of SIRT3 and MAVS. H1299 cells were transfected with Flag-SIRT3 for 24 h, followed by UI or infected with VSV for 6 h. Confocal microscopy image of Flag-SIRT3 was detected by immunofluorescence staining with anti-Flag antibody, and endogenous MAVS was detected by immunofluorescence staining with anti-MAVS antibody, (Scale bar, 10 μm.) (*E*) H1299 cells were transfected with Flag-SIRT3 or Flag empty vector as control for 24 h, followed by UI (−) or infected with VSV (+) infection for 6 h. In situ PLAs of the SIRT3-MAVS interaction in H1299 cells with indicated combinations using anti-Flag and anti-MAVS antibodies. Quantification analysis of the SIRT3-MAVS interaction is shown in the *Right* figure. (Scale bar, 25 μm.) (*F* and *G*) qPCR analysis of *IFNβ* (*F*) and *CXCL10* (*G*) mRNA in A549 cells stably expressing empty vector, SIRT3, or the enzymatically inactive mutant SIRT3-H248Y (lentivirus infection), followed by infection without (UI) or with VSV for 8 h. (*H–J*) A549 cells stably expressing empty vector, SIRT3, or the enzymatically inactive mutant SIRT3-H248Y were infected with VSV-GFP virus (MOI = 0.1) for 16 h, and viral infectivity was detected by flow cytometry analysis (n = 3) (*H*), fluorescence microscopy (*I*), or IB (*J*). (*K* and *L*) qPCR analysis of *IFNβ* (*K*) and *CXCL10* (*L*) mRNA in *SIRT3*-deficient A549 cells (*SIRT3*$^{-/-}$) transfected with empty vector, Myc-tagged SIRT3 or the enzymatically inactive mutant SIRT3-H248Y for 24 h, followed by UI or infected with VSV for 8 h. **P* < 0.05, ***P* < 0.01, ****P* < 0.001, *****P* < 0.0001. Data from at least three independent experiments (mean ± SD) (*E–H*, *K*, and *L*).

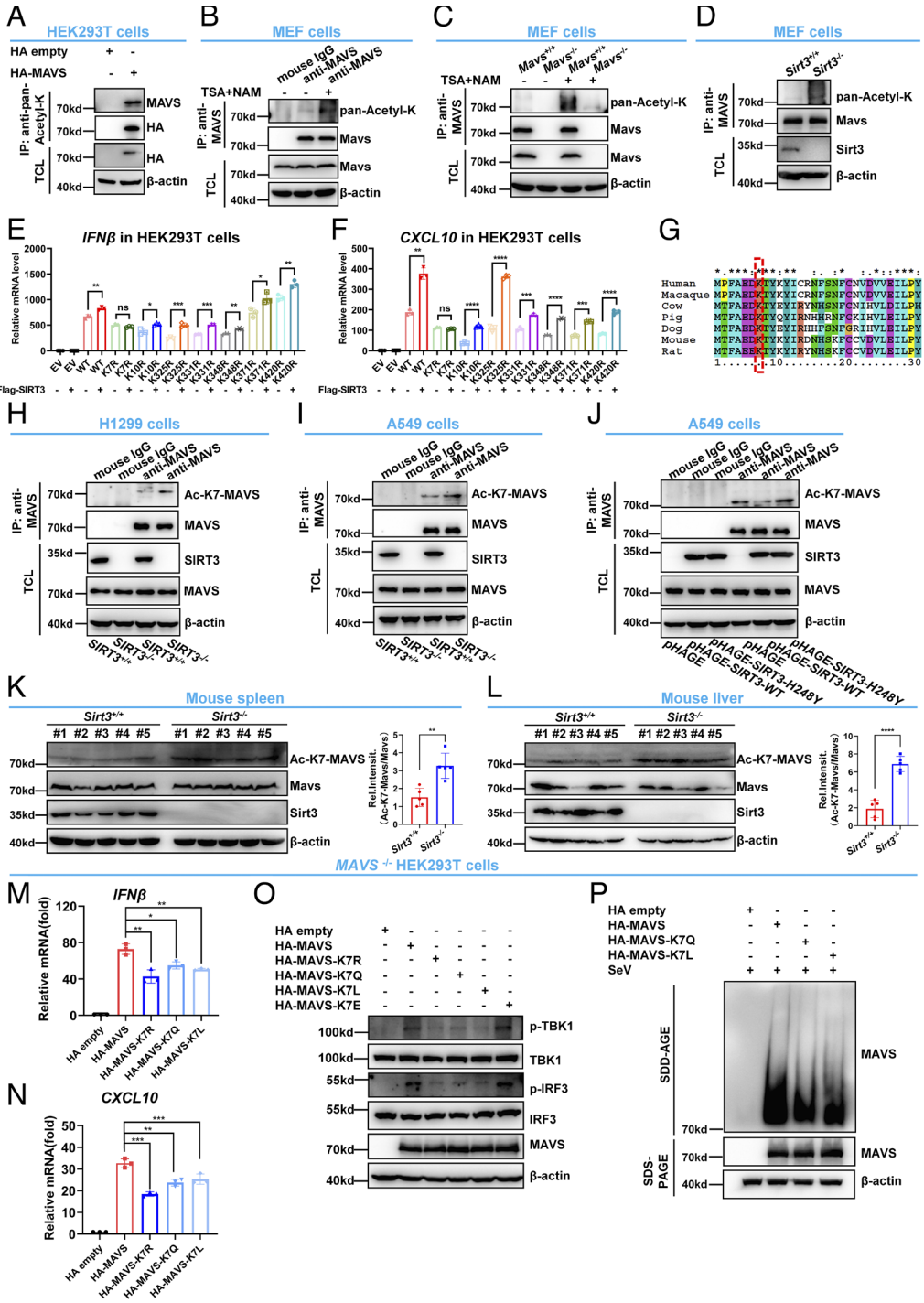

Fig. 3. SIRT3 deacetylates MAVS at lysine 7. (*A*) HEK293T cells were transfected with HA empty vector (HA empty) or HA-MAVS for 24 h. Anti-pan-acetyl-K antibody was used for IP, followed by immunoblotting with anti-MAVS antibody. (*B*) MEF cell lysates were immunoprecipitated with anti-MAVS antibody or mouse IgG control, followed by immunoblotting with anti-pan-acetyl-K antibody. (*C*) *Mavs*$^{-/-}$ or *Mavs*$^{+/+}$ MEF cells were treated with (+) or without (−) TSA and NAM for 4 h, and the cell lysates were immunoprecipitated with anti-MAVS antibody, followed by immunoblotting with anti-pan-Acetyl-K antibody. (*D*) Cell lysates from *Sirt3*$^{-/-}$ or *Sirt3*$^{+/+}$ MEF cells were immunoprecipitated with anti-MAVS antibody, followed by immunoblotting with anti-pan-Acetyl-K antibody. (*E* and *F*) qPCR analysis of *IFNβ* (*E*) and *CXCL10* (*F*) mRNA in HEK293T cells transfected with HA-MAVS WT or mutants together with (+) or without (−) Flag-*SIRT3* for 24 h. EV, empty vector. (*G*) Sequence alignment of partial MAVS (1 to 30 amino acids) from the human, macaque, cow, pig, dog, mouse, and rat. The red box indicates the conserved lysine 7 (K7). (*H*) Cell lysates from *SIRT3*$^{-/-}$ or *SIRT3*$^{+/+}$ H1299 cells were immunoprecipitated with anti-MAVS antibody or mouse IgG control, followed by immunoblotting with anti-Ac-K7-MAVS antibody. (*I*) Cell lysates from *SIRT3*$^{-/-}$ or SIRT3$^{+/+}$ A549 cells were immunoprecipitated with anti-MAVS antibody or mouse IgG control, followed by IB with anti-Ac-K7-MAVS antibody. (*J*) Cell lysates from A549 cells stably expressing empty vector, SIRT3, or the enzymatically inactive mutant SIRT3-H248Y were immunoprecipitated with anti-MAVS antibody or mouse IgG control, followed by immunoblotting with anti-Ac-K7-MAVS antibody. (*K* and *L*) Disruption of *Sirt3* in mice increased MAVS acetylation in mouse spleen (*K*) and liver (*L*). Proteins extracted from spleens (*K*) and livers (*L*) of *Sirt3*$^{-/-}$ or *Sirt3*$^{+/+}$ littermates (n = 5 per group) were analyzed with the indicated antibodies. MAVS acetylation was determined using anti-Ac-K7-MAVS antibody. Relative acetylation levels were quantified (*Right*). (*M* and *N*) qPCR analysis of *IFNβ* (*M*) and *CXCL10* (*N*) mRNA in *MAVS*$^{-/-}$ HEK293T cells transfected with HA-MAVS, or its acetylation-deficient mutant (HA-MAVS-K7R), or its acetylation mimic-mutant (HA-MAVS-K7Q or HA-MAVS-K7L) for 24 h. (*O*) IB of TBK1 and IRF3 phosphorylation in *MAVS*$^{-/-}$ HEK293T cells transfected with HA-MAVS, or its acetylation-deficient mutant (HA-MAVS-K7R), or its acetylation mimic-mutant (HA-MAVS-K7Q or HA-MAVS-K7L), or its succinylation mimic-mutant (HA-MAVS-K7E) for 24 h. (*P*) SDD-AGE analysis of MAVS aggregates in *MAVS*$^{-/-}$ HEK293T cells transfected with HA-MAVS or its acetylation-mimic mutant (HA-MAVS-K7Q or HA-MAVS-K7L) for 24 h, followed by infection with SeV for 12 h. SDS–PAGE immunoblotting was used as a loading control. ns, not significant ($P > 0.05$), *$P < 0.05$, **$P < 0.01$, ***$P < 0.001$, ****$P < 0.0001$. Data from at least three independent experiments (mean ± SD) (*E*, *F*, and *K*–*N*).

7 of MAVS may be specifically targeted by SIRT3 to mediate the enhancing effect of SIRT3 on RLR signaling (Fig. 3 *E–G*).

Subsequently, we developed a specific antibody against lysine 7 of MAVS (anti-Ac-K7-MAVS antibody). The specificity of this antibody was validated by dot blot assay (*SI Appendix*, Fig. S6*B*). When WT (HA-MAVS) or mutant MAVS (HA-MAVS-K7R) was ectopically expressed in HEK293T cells, only WT MAVS could be detected by the anti-Ac-K7-MAVS antibody in the precipitate obtained with anti-HA conjugated agarose beads (*SI Appendix*, Fig. S6*C*), confirming the specificity of the antibody. After Co-IP with anti-MAVS antibody, we found that MAVS acetylation at lysine 7 was much higher in *SIRT3*-deficient H1299 cells ($SIRT3^{-/-}$) than in WT H1299 cells ($SIRT3^{+/+}$), as revealed by anti-Ac-K7-MAVS antibody (Fig. 3*H*). Similar results were observed in $SIRT3^{+/+}$ and $SIRT3^{-/-}$ A549 cells (Fig. 3*I*). Furthermore, in A549 cells, overexpression of WT SIRT3 (pHAGE-SIRT3-WT) reduced MAVS acetylation at lysine 7, whereas overexpression of the enzymatically inactive mutant of SIRT3 (pHAGE-SIRT3-H248Y) did not (Fig. 3*J*). As expected, the addition of 3-TYP restored the acetylation of MAVS (*SI Appendix*, Fig. S6 *D* and *E*).

To further determine the function of *SIRT3* in vivo, we generated *Sirt3*-knockout mice using CRISPR/Cas9 technology (*SI Appendix*, Fig. S7*A*). *Sirt3* deficiency in mice not only did not affect general development, but also did not affect immune cell development as previously reported (*SI Appendix*, Fig. S7 *B* and *C*) (32). However, MAVS acetylation at lysine 7 in the spleen and liver was significantly increased in $Sirt3^{-/-}$ mice compared to $Sirt3^{+/+}$ mice as revealed by anti-Ac-K7-MAVS antibody, confirming the effect of Sirt3 on Mavs deacetylation at lysine 7 in vivo (Fig. 3 *K* and *L*). To validate the importance of lysine 7 acetylation in affecting MAVS activation, we generated two acetylation mimic mutants of MAVS, MAVS-K7L, and MAVS-K7Q (33). In $MAVS^{-/-}$ HEK293T cells, the enhancement of MAVS-K7L on the expression of *IFNβ* and *CXCL10* was significantly lower than that of WT MAVS (Fig. 3 *M* and *N*). Consistent with these findings, the phosphorylation of IRF3 (p-IRF3) and TBK1 (p-TBK1) induced by ectopic expression of MAVS-K7L and MAVS-K7Q in $MAVS^{-/-}$ HEK293T cells was much weaker than that induced by ectopic expression of WT MAVS (Fig. 3*O*). The aggregates formed by MAVS-K7L and MAVS-K7Q were also much weaker than those formed by WT MAVS (Fig. 3*P*). Unexpectedly, the induction of *IFNβ* and *CXCL10* expression and phosphorylation of IRF3 (p-IRF3) and TBK1 (p-TBK1), as well as aggregate formation, by ectopic expression of MAVS-K7R were weaker than those by ectopic expression of WT MAVS (Fig. 3 *M–O* and *SI Appendix*, Fig. S8*A*), which may be due to the simultaneous loss of multiple modifications in MAVS-K7R (15, 22, 34). In contrast to MAVS-K7L and MAVS-K7Q, phosphorylation of IRF3 (p-IRF3) and TBK1 (p-TBK1) and aggregate formation were much stronger upon ectopic expression of MAVS-K7E, a succinylation mimic mutant of MAVS, was much stronger (Fig. 3*O* and *SI Appendix*, Fig. S8*B*). In addition, SIRT3 overexpression or knockout had no obvious effect on SIRT5 protein levels (*SI Appendix*, Fig. S8 *C* and *D*).

These data suggest that SIRT3 targets MAVS at lysine 7 to deacetylate MAVS, leading to the enhancement of MAVS activation in RLR signaling.

Disruption of *Sirt3* in Mice Attenuates the Cellular Antiviral Immune Response in MEF, BMDC, and BoneMarrow-Derived Macrophages (BMDM) Cells. To determine the effects of *Sirt3* on innate immunity in vivo, we used *Sirt3*-deficient mice. First, we established MEF cell lines from WT mice ($Sirt3^{+/+}$) and *Sirt3*-deficient mice ($Sirt3^{-/-}$) and challenged them with SeV or VSV. Compared to $Sirt3^{+/+}$ MEF cells, the expression of *Ifnβ, Cxcl10, Cxcl11, Isg15, Ccl5, Rig-I,* or *Ifit1* mRNA was significantly reduced in $Sirt3^{-/-}$ MEF cells upon SeV or VSV challenge (*SI Appendix*, Fig. S9 *A–J*). Consistent with this, *Sirt3* deficiency attenuated the formation of Mavs aggregates in response to SeV infection (*SI Appendix*, Fig. S9*K*). Furthermore, phosphorylation of Irf3 and Tbk1 was impaired in $Sirt3^{-/-}$ MEF cells compared to $Sirt3^{+/+}$ MEF cells upon VSV infection (*SI Appendix*, Fig. S9 *L* and *M*). In contrast, VSV-GFP virus propagation was enhanced in $Sirt3^{-/-}$ MEF cells as shown by fluorescence microscopy imaging and immunoblotting (*SI Appendix*, Fig. S9*N*). Similarly, the expression of *Ifnβ, Cxcl10, Isg15,* or *Ifit1* mRNA was significantly decreased in $Sirt3^{-/-}$ MEF cells when transfected with poly (I:C) HMW or LMW compared with that in $Sirt3^{+/+}$ MEF cells (*SI Appendix*, Fig. S9 *O–R*). As expected, the Ifnβ levels were lower in $Sirt3^{-/-}$ MEF cells compared to $Sirt3^{+/+}$ MEF cells after transfection with poly (I:C) LMW (*SI Appendix*, Fig. S9*S*). Similar results were obtained by infection with encephalomyocarditis virus (EMCV) (*SI Appendix*, Fig. S9 *T–X*). In $Sirt3^{-/-}$ MEF cells, treatment with 3-TYP had no apparent effect on the expression of *Ifnβ* and *Isg15* upon EMCV infection (*SI Appendix*, Fig. S9 *Y* and *Z*).

To further validate the above observations, we established both bone marrow-derived dendritic cells (BMDCs) and BMDMs and performed similar experiments. SeV- and VSV-induced expression of *Ifnβ, Isg15, Ifit1, Rig-I*, and *Ccl5* mRNA was attenuated in $Sirt3^{-/-}$ BMDC compared to $Sirt3^{+/+}$ BMDC upon SeV or VSV infection (*SI Appendix*, Fig. S10 *A–J*). Consistent with these findings, phosphorylation of Irf3 and Tbk1 was impaired in $Sirt3^{-/-}$ BMDCs compared to that in $Sirt3^{+/+}$ BMDCs upon SeV or VSV infection (*SI Appendix*, Fig. S10 *K–N*). Similar results were obtained in $Sirt3^{+/+}$ and $Sirt3^{-/-}$ BMDM cells upon SeV or VSV infection (*SI Appendix*, Fig. S10 *O–Y*).

Taken together, these data suggest that disruption of *Sirt3* attenuates the cellular antiviral innate immune response.

***Sirt3*-Deficient Mice Are More Susceptible to Viral Infections.** After intraperitoneal injection (i.p.) of VSV, acetylation of MAVS in the spleen and liver of $Sirt3^{-/-}$ mice was significantly higher than that of $Sirt3^{+/+}$ mice as detected by anti-Ac-K7-MAVS antibody (Fig. 4 *A* and *B*). As expected, the expression of *Ifnβ*, *Ifnα1, Ifnα4, Cxcl10, Cxcl11, Ifit1, Isg15,* or *Rig-I* mRNA was attenuated in the spleen, lung, and liver of $Sirt3^{-/-}$ mice compared to those of $Sirt3^{+/+}$ mice after i.p. injection of VSV (Fig. 4 *C–T*).

Consistent with these findings, $Sirt3^{-/-}$ mice were more susceptible to VSV infection than $Sirt3^{+/+}$ mice (Fig. 4*U*). Serum Ifnβ levels were lower in $Sirt3^{-/-}$ mice than in $Sirt3^{+/+}$ mice (Fig. 4*V*). Hematoxylin and eosin (H&E) staining revealed more immune cell infiltration and injury in the lungs of $Sirt3^{-/-}$ mice compared to $Sirt3^{+/+}$ mice (Fig. 4*W*). In contrast, VSV propagation was enhanced in $Sirt3^{-/-}$ BMDC compared to $Sirt3^{+/+}$ BMDC (*SI Appendix*, Fig. S11 *A* and *B*). Similar results were observed in the spleen, liver, and lung of $Sirt3^{-/-}$ mice compared to $Sirt3^{+/+}$ mice (*SI Appendix*, Fig. S11 *C–E*). In addition, the body weight of $Sirt3^{-/-}$ mice was lower than that of $Sirt3^{+/+}$ mice after VSV infection for 6 d (*SI Appendix*, Fig. S11*F*).

Furthermore, after i.p. injection of EMCV, an ssRNA virus specifically sensed by MDA5 (Fig. 4*X*) (35), the expression of *Ifnβ*, *Cxcl10*, and *Isg15* mRNA was reduced in the spleen, lung, and liver of $Sirt3^{-/-}$ mice, compared to those of $Sirt3^{+/+}$ mice (Fig. 4 *Y* and *Z* and *SI Appendix*, Fig. S11 *G–L*).

These data suggest that *Sirt3* is an important positive regulator of innate immunity against RNA viruses in vivo.

***sirt3*-Deficient Zebrafish Are More Susceptible to Viral Infection.** By comparing the amino acid sequences between different organisms, we found that SIRT3 is evolutionarily conserved, particularly in the C-terminus of SIRT3 (*SI Appendix*, Fig. S12*A*). To validate the general

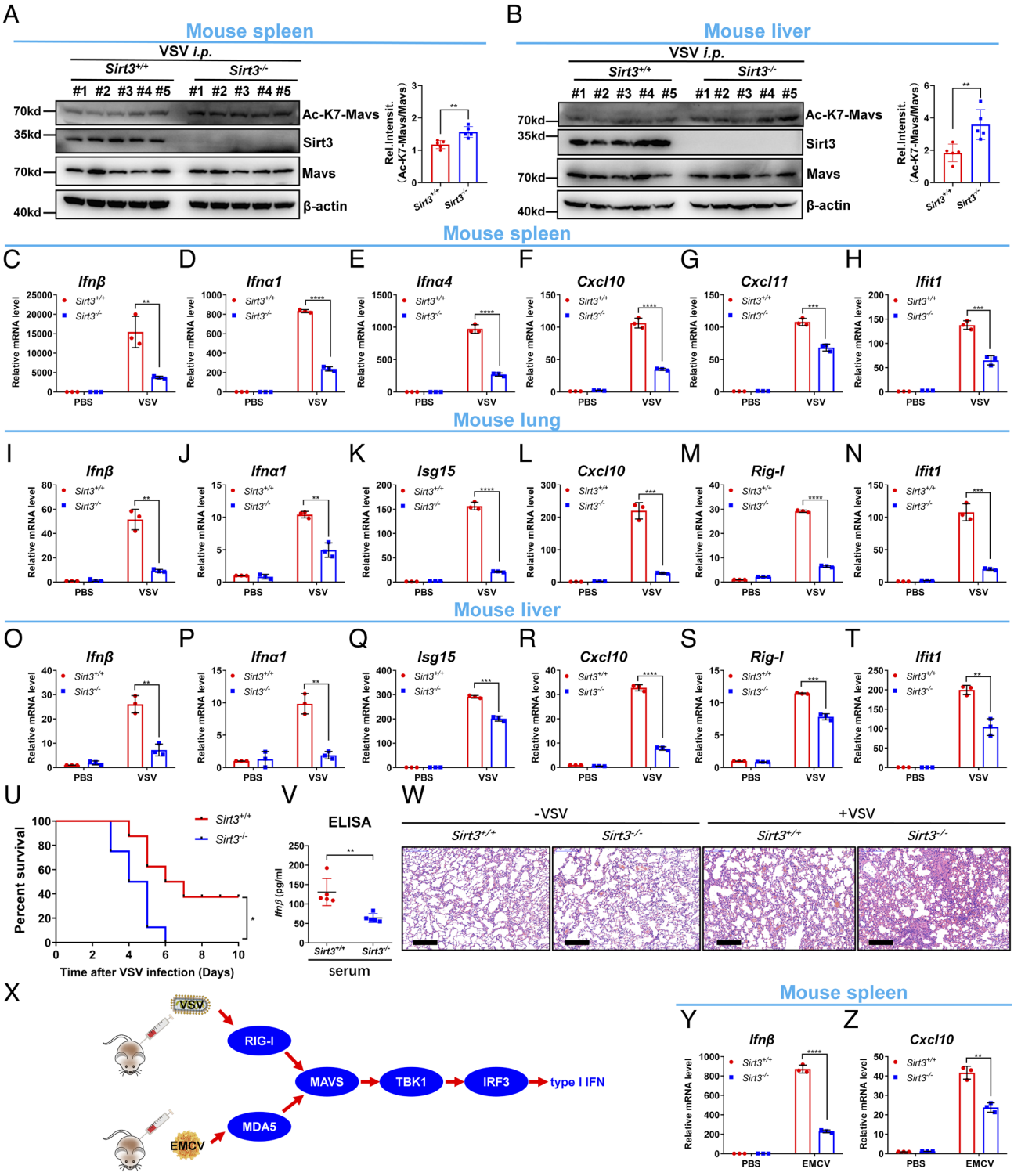

Fig. 4. *Sirt3*-deficient mice are more susceptible to viral infection. (*A*) Disruption of *Sirt3* in mice increased MAVS acetylation in mouse spleen upon VSV infection. Proteins extracted from spleens of $Sirt3^{-/-}$ and $Sirt3^{+/+}$ littermates injected intraperitoneally with VSV [3×10^7 plaque-forming units (PFU) per mouse] for 24 h (n = 5 per group) were analyzed with the indicated antibodies. MAVS acetylation was detected by anti-Ac-K7-MAVS antibody and the relative acetylation level was quantified. (*B*) Disruption of *Sirt3* in mice increased MAVS acetylation in mouse liver after VSV infection. Proteins extracted from livers of $Sirt3^{-/-}$ and $Sirt3^{+/+}$ littermates injected intraperitoneally with VSV [3×10^7 PFU per mouse] for 24 h (n = 5 per group) were analyzed with the indicated antibodies. MAVS acetylation was detected by anti-Ac-K7-MAVS antibody and the relative acetylation level was quantified. (*C*–*H*) qPCR analysis of *Ifnβ* (*C*), *Ifnα1* (*D*), *Ifnα4* (*E*), *Cxcl10* (*F*), *Cxcl11* (*G*), and *Ifit1* (*H*) mRNA in the spleens of $Sirt3^{-/-}$ and $Sirt3^{+/+}$ mice injected intraperitoneally with VSV (3×10^7 PFU per mouse) or PBS control for 24 h. (*I*–*N*) qPCR analysis of *Ifnβ* (*I*), *Ifnα1* (*J*), *Isg15* (*K*), *Cxcl10* (*L*), *Rig-I* (*M*), and *Ifit1* (*N*) mRNA in the lungs of $Sirt3^{-/-}$ and $Sirt3^{+/+}$ mice injected intraperitoneally with VSV (3×10^7 PFU per mouse) or PBS control for 24 h. (*O*–*T*) qPCR analysis of *Ifnβ* (*O*), *Ifnα1* (*P*), *Isg15* (*Q*), *Cxcl10* (*R*), *Rig-I* (*S*), and *Ifit1* (*T*) mRNA in the livers of $Sirt3^{-/-}$ and $Sirt3^{+/+}$ mice injected intraperitoneally with VSV (3×10^7 PFU per mouse) or PBS control for 24 h. (*U*) Survival (Kaplan–Meier curve) of $Sirt3^{-/-}$ and $Sirt3^{+/+}$ mice (n = 8) injected intraperitoneally with a high dose of VSV (3×10^7 PFU per mouse) and monitored for 10 d. $^*P < 0.05$, using the log-rank test (Mantel-Cox). (*V*) ELISA of Ifnβ in serum from the $Sirt3^{-/-}$ (n = 5) and $Sirt3^{+/+}$ mice (n = 5) injected intraperitoneally with VSV (3×10^7 PFU per mouse) or PBS control for 24 h. (*W*) Hematoxylin-and-eosin-stained (H&E) images of lung sections from mice in (*V*). (Scale bar, 50 μm.) (*X*) Schematic of the working model for two RNA viruses, VSV and EMCV. (*Y* and *Z*) qPCR analysis of *Ifnβ* (*Y*) and *Cxcl10* (*Z*) mRNA in the spleens of $Sirt3^{-/-}$ and $Sirt3^{+/+}$ mice injected intraperitoneally with EMCV (1×10^6 PFU per mouse) or PBS control for 24 h. ns, not significant ($P > 0.05$), $^*P < 0.05$, $^{**}P < 0.01$, $^{***}P < 0.001$, $^{****}P < 0.0001$. Data from at least three independent experiments (mean ± SD) (*A*–*T*, *V*, *Y*, and *Z*).

role of *SIRT3* in antiviral innate immunity, we used the zebrafish model to perform additional assays (36). Upon infection of Epithelioma papulosum cyprini (EPC) cells with spring viremia of carp virus (SVCV, a single-strand RNA virus of fish) (37), overexpression of zebrafish *sirt3* enhanced the expression of *ifn, isg15,* and *viperin* mRNA, similar to that was observed in mammalian models (*SI Appendix*, Fig. S12 *B–D*). In addition, zebrafish mavs interacted with zebrafish sirt3 when overexpressed (*SI Appendix*, Fig. S12*E*).

Using CRISPR/Cas9, we generated a mutant line with ten nucleotides deleted in exon 4 of zebrafish *sirt3* (*SI Appendix*, Fig. S12*F*). After adding SVCV to the water containing zebrafish larvae (3 days post fertilization [dpf]) for 27 h, we found that *sirt3*-deficient zebrafish larvae ($sirt3^{-/-}$) were more susceptible to SVCV-induced death compared to WT zebrafish larvae ($sirt3^{+/+}$) (*SI Appendix*, Fig. S12 *G* and *H*). Similar results were obtained when WT zebrafish larvae ($sirt3^{+/+}$) and *sirt3*-deficient zebrafish larvae ($sirt3^{-/-}$) were infected with grass carp reovirus (GCRV), a double-stranded RNA virus (38) (*SI Appendix*, Fig. S12 *I* and *J*).

Next, we sought to determine whether zebrafish *sirt3* function is dependent on its enzymatic activity using the SIRT3 inhibitor, 3-TYP. In zebrafish ZFL cells, upon SVCV infection or poly (I:C) transfection, the addition of 3-TYP significantly reduced the expression of *ifnφ1, lta,* and *mxc* mRNA (*SI Appendix*, Fig. S13 *A–I*). Furthermore, in zebrafish larvae (3 dpf), the addition of 3-TYP also significantly reduced the expression of *ifnφ1, lta,* and *mxc* mRNA upon SVCV infection (*SI Appendix*, Fig. S13 *J–L*). As expected, the addition of 3-TYP to the water containing zebrafish larvae (3 dpf) promoted SVCV-induced death (*SI Appendix*, Fig. S13 *M* and *N*).

Taken together, these data suggest that zebrafish *sirt3* also positively regulates antiviral innate immunity, in a manner dependent on its enzymatic activity.

Disruption of *Sirt5* in *Sirt3*-Deficient Mice Counteracts the Increased Viral Susceptibility Exhibited by *Sirt3*-Deficient Mice. Interestingly, the same lysine of MAVS (lysine 7) can not only be modified simultaneously by SIRT3 and SIRT5, but also has opposing effects on MAVS activation (22). Notably, $Sirt5^{-/-}$ mice are more resistant to viral infection (22), whereas $Sirt3^{-/-}$ mice are more susceptible to viral infection. These phenomena led us to hypothesize that deacetylation of MAVS at lysine 7 by SIRT3 may act as an accelerator, but desuccinylation of MAVS at lysine 7 by SIRT5 may act as a brake in RLR signaling. To test this hypothesis, we generated *Sirt3* and *Sirt5* double knockout mice by crossing $Sirt3^{+/-}Sirt5^{+/-}$ (♀) mice × $Sirt3^{+/-}Sirt5^{+/-}$ (♂) mice (Fig. 5*A*). As previously reported, $Sirt3^{-/-}Sirt5^{-/-}$ mice reproduced and developed without abnormalities, as well as their immune cell development was normal (*SI Appendix*, Fig. S14 *A* and *B*) (39). In BMDCs, SeV- and VSV-induced *Ifnβ* expression was quite similar between $Sirt3^{-/-}Sirt5^{-/-}$ mice and their WT littermates ($Sirt3^{+/+}Sirt5^{+/+}$) (Fig. 5 *B* and *C*). Consistent with this, the level of Ifnβ in the supernatants was also similar between $Sirt3^{-/-}Sirt5^{-/-}$ BMDC and their WT BMDCs ($Sirt3^{+/+}Sirt5^{+/+}$) (Fig. 5*D*).

Furthermore, we observed that the phosphorylation of Irf3 and Tbk1 induced by VSV infection in BMDCs was almost the same between $Sirt3^{-/-}Sirt5^{-/-}$ mice and their WT littermates ($Sirt3^{+/+}Sirt5^{+/+}$) (Fig. 5 *E* and *F*). Consistent with these findings, upon VSV infection, the expression of *Ifnβ, Isg15,* and *Cxcl10* mRNA in the spleen, lung, and liver of $Sirt3^{-/-}Sirt5^{-/-}$ mice was the same as that of $Sirt3^{+/+}Sirt5^{+/+}$ mice (Fig. 5 *G–O*).

In addition, upon EMCV infection, the expression of *Ifnβ, Isg15,* and *Cxcl10* mRNA in the spleen, lung, and liver of $Sirt3^{-/-}Sirt5^{-/-}$ mice was also the same as that of $Sirt3^{+/+}Sirt5^{+/+}$ mice (Fig. 5 *P–W*). As expected, EMCV-induced death was the same between $Sirt3^{-/-}Sirt5^{-/-}$ mice and $Sirt3^{+/+}Sirt5^{+/+}$ mice (Fig. 5*X*). Taken together, these data suggest that the double knockout of *Sirt5* and *Sirt3* counteracts the enhancement of antiviral innate immunity by loss of *Sirt5* as well as the impairment of antiviral innate immunity by loss of *Sirt3*, resulting in complete rescue of single mutant phenotypes exhibited in either $Sirt3^{-/-}$ mice or $Sirt5^{-/-}$ mice in response to viral infection.

This phenomenon prompted us to look closely at the underlying mechanisms. Notably, succinylation of lysine changes the charge of lysine from "+1" to "−1," whereas acetylation of lysine changes the charge of lysine from "+1" to "0" (*SI Appendix*, Fig. S14*C*). It appears that succinylation of lysine reverses the charge in lysine, but acetylation of lysine neutralizes the charge in lysine. Thus, succinylation of the protein may strengthen its binding to its oppositely charged partners, but acetylation of the protein may weaken its binding to its partners due to its charge neutralization. Based on the structure of MAVS complexed with RIG-I, the tandem CARDs of RIG-I [2CARD (RIG-I)] tightly interact with the CARD of MAVS, leading to CARD (MAVS) filament assembly and activation of interferon signaling (*SI Appendix*, Fig. S14 *D* and *E*) (40). Structural modeling of MAVS succinylation and acetylation at lysine 7 shows that acetylation at K7 results in a longer distance between MAVS and the components of the MAVS/RIG-I complex (9.4, 6.8, and 7.5 versus 3.9, 6.8, and 6.7) compared to succinylation at K7 (*SI Appendix*, Fig. S14 *D* and *E*). Therefore, acetylation of MAVS at lysine 7 may weaken its binding to RIG-I, resulting in impaired RLR signaling.

In WT MEF cells, MAVS acetylation and succinylation were maintained at relatively uniform levels upon VSV infection (Fig. 5 *Y* and *Z*). In $Sirt5^{-/-}$ MEF cells, upon VSV infection, MAVS succinylation was enhanced, but MAVS acetylation was maintained at a very low level (Fig. 5 *Y* and *Z*). Conversely, in $Sirt3^{-/-}$ MEF cells, upon VSV infection, MAVS acetylation was enhanced, but MAVS succinylation remained at a very low level (Fig. 5 *Y* and *Z*). However, upon VSV infection, it appeared that both MAVS acetylation and MAVS succinylation in $Sirt3^{-/-}Sirt5^{-/-}$ MEF cells were similar to those in $Sirt3^{+/+}Sirt5^{+/+}$MEF cells (Fig. 5 *Y* and *Z*). These data suggest that MAVS acetylation and succinylation at lysine 7 might interfere with each other.

Based on our observations, we proposed a working model for the control of MAVS activation by SIRT3-mediated deacetylation and SIRT5-mediated desuccinylation (*SI Appendix*, Fig. S15).

Discussion

In this study, we show that two different modifications on the same lysine of MAVS have opposing effects on MAVS-mediated antiviral innate immunity, revealing a previously unrecognized mechanism for orchestrating innate immunity. However, how these two modifications dynamically change and cooperate to exert their functions in maintaining immune homeostasis during both resting states and pathogen infection remains a mystery. Of note, it appears that acetylation can interfere with succinylation on lysine 7 of MAVS and vice versa during viral infection, thus, the dual modification on lysine 7 of MAVS may cooperate to regulate MAVS function in the RLR signaling.

As reported, SIRT3 is a primarily mitochondrial matrix protein and lysine 7 of MAVS is in the cytoplasm (41–44). If SIRT3 can modify MAVS, then lysine 7 of MAVS should be accessible to SIRT3. Although we have tested several commercially available anti-SIRT3 antibodies, none of them can detect endogenous SIRT3 localization by immunofluorescence staining. Thus, we could not directly observe that endogenous SIRT3 can colocalize with endogenous MAVS. In this study, we show that endogenous SIRT3 coimmunoprecipitates with endogenous MAVS. In addition, we show that overexpressed SIRT3 at comparable endogenous levels

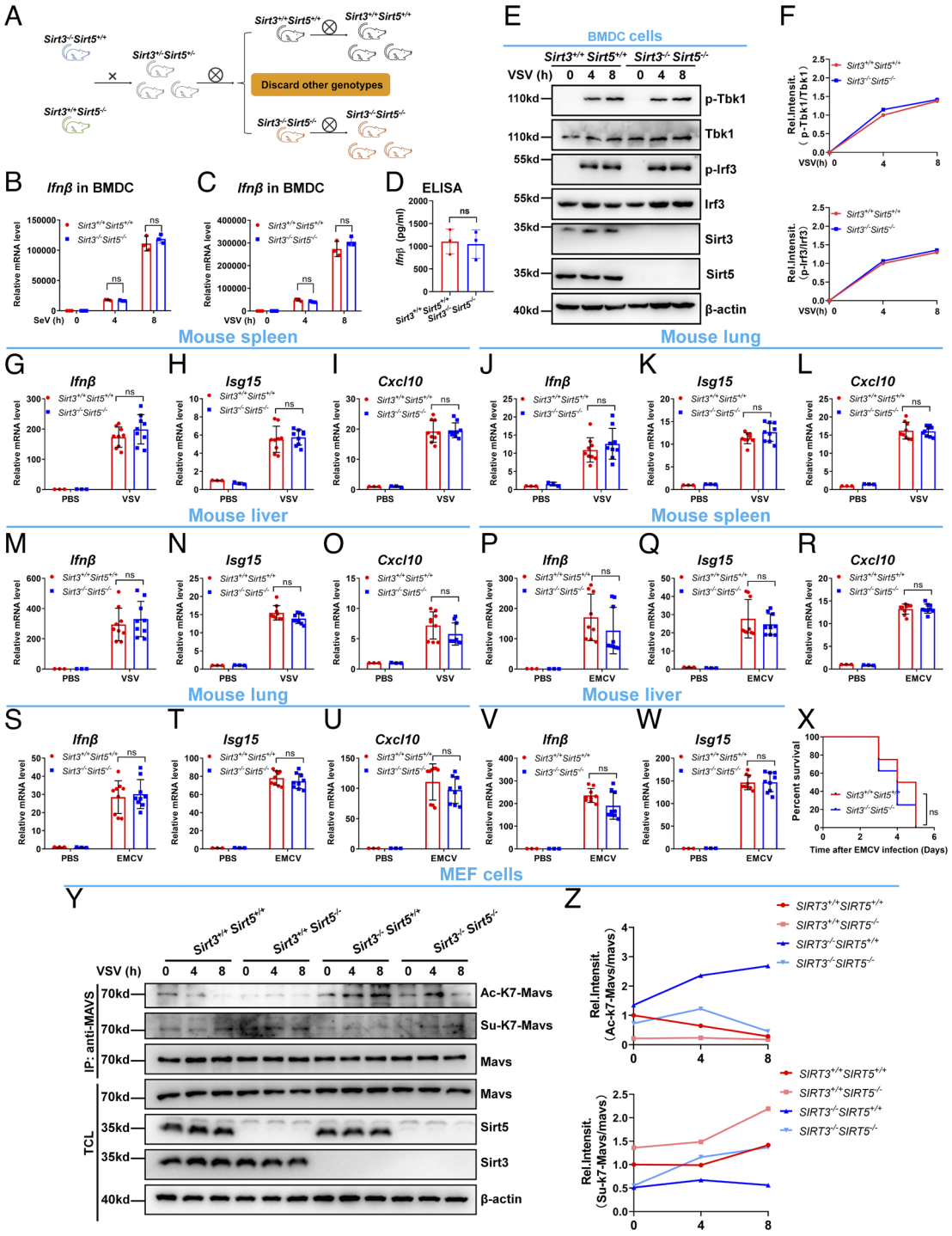

Fig. 5. Disruption of *Sirt5* in *Sirt3*-deficient mice counteracts the viral susceptibility exhibited in *Sirt3*-deficient mice. (*A*) Schematic of generation of *Sirt3* and *Sirt5* double knockout mice ($Sirt3^{-/-}Sirt5^{-/-}$). (*B*) qPCR analysis of *Ifnβ* mRNA in $Sirt3^{-/-}Sirt5^{-/-}$ or $Sirt3^{+/+}Sirt5^{+/+}$ BMDCs infected without (0) or with SeV for 4 h or 8 h. (*C*) qPCR analysis of *Ifnβ* mRNA in $Sirt3^{-/-}Sirt5^{-/-}$ or $Sirt3^{+/+}Sirt5^{+/+}$ BMDCs infected without (0) or with VSV for 4 h or 8 h. (*D*) ELISA of Ifnβ in supernatants of $Sirt3^{-/-}Sirt5^{-/-}$ or $Sirt3^{+/+}Sirt5^{+/+}$ BMDCs infected with VSV for 12 h. (*E*) IB of Tbk1 and Irf3 phosphorylation in $Sirt3^{-/-}Sirt5^{-/-}$ or $Sirt3^{+/+}Sirt5^{+/+}$ BMDCs infected without (0) or with VSV for 4 h or 8 h. (*F*) Quantitation of phosphorylated Tbk1 (p-Tbk1) and Irf3 (p-Irf3) proteins shown in (*E*). (*G–I*) qPCR analysis of *Ifnβ* (*G*), *Isg15* (*H*), and *Cxcl10* (*I*) mRNA in the spleens of $Sirt3^{-/-}Sirt5^{-/-}$ or $Sirt3^{+/+}Sirt5^{+/+}$ mice injected intraperitoneally with VSV (3×10^7 PFU per mouse) or PBS control for 24 h. (*J–L*) qPCR analysis of *Ifnβ* (*J*), *Isg15* (*K*), and *Cxcl10* (*L*) mRNA in the lungs of $Sirt3^{-/-}Sirt5^{-/-}$ or $Sirt3^{+/+}Sirt5^{+/+}$ mice injected intraperitoneally with VSV (3×10^7 PFU per mouse) or PBS control for 24 h. (*M–O*) qPCR analysis of *Ifnβ* (*M*), *Isg15* (*N*), and *Cxcl10* (*O*) mRNA in the livers of $Sirt3^{-/-}Sirt5^{-/-}$ or $Sirt3^{+/+}Sirt5^{+/+}$ mice injected intraperitoneally with VSV (3×10^7 PFU per mouse) or PBS control for 24 h. (*P–R*) qPCR analysis of *Ifnβ* (*P*), *Isg15* (*Q*), and *Cxcl10* (*R*) mRNA in the spleens of $Sirt3^{-/-}Sirt5^{-/-}$ and $Sirt3^{+/+}Sirt5^{+/+}$ mice injected intraperitoneally with EMCV (1×10^6 PFU per mouse) or PBS control for 24 h. (*S–U*) qPCR analysis of *Ifnβ* (*S*), *Isg15* (*T*), and *Cxcl10* (*U*) mRNA in the lungs of $Sirt3^{-/-}Sirt5^{-/-}$ and $Sirt3^{+/+}Sirt5^{+/+}$ mice injected intraperitoneally with EMCV (1×10^6 PFU per mouse) or PBS control for 24 h. (*V* and *W*) qPCR analysis of *Ifnβ* (*V*) and *Isg15* (*W*) mRNA in the livers of $Sirt3^{-/-}Sirt5^{-/-}$ and $Sirt3^{+/+}Sirt5^{+/+}$ mice injected intraperitoneally with EMCV (1×10^6 PFU per mouse) or PBS control for 24 h. (*X*) Survival (Kaplan–Meier curve) of $Sirt3^{-/-}Sirt5$ (n = 8) and $Sirt3^{+/+}Sirt5^{+/+}$ mice (n = 8) injected intraperitoneally with a high dose of EMCV (1×10^6 PFU per mouse) and monitored for 6 d. ns, not significant ($P > 0.05$). (*Y*) The dynamic changes of acetylation and succinylation of MAVS at lysine 7 in response to VSV infection in $Sirt3^{+/+}Sirt5^{+/+}$, $Sirt5^{-/-}$, $Sirt3^{-/-}$, and $Sirt3^{-/-}Sirt5^{-/-}$ MEF cells. MEF cells were infected with VSV for the indicated time points, and then cell lysates were immunoprecipitated with anti-MAVS antibody, followed by immunoblotting with the indicated antibodies. (*Z*) Quantitation of acetylated MAVS (Ac-K7-Mavs) and succinylated MAVS (Su-K7-Mavs) proteins shown in (*Y*). ns, not significant ($P > 0.05$). Data are from at least three independent experiments (mean ± SD) (*B–D* and *G–W*).

colocalizes with TOM2O, an outer mitochondrial membrane protein upon viral infection. Furthermore, SIRT3 colocalizes with MAVS during viral infection. Indeed, SIRT3 has been reported to localize to other parts of the cell in addition to the mitochondrial matrix under various circumstances. Thus, SIRT3 may translocate to the outer mitochondrial membrane to interact with and modify MAVS in response to viral infection. Similar behaviors may also exist for SIRT5, which is predominantly localized to the mitochondria, but also exerts regulatory activity in the cytoplasm (45–47).

The N-terminal CARD (from 10 to 93 amino acids) is the key domain for MAVS aggregation and subsequent activation (44, 48, 49). However, lysine 7 is close to the CARD, but not exactly localized to it. Both deacetylation and desuccinylation of MAVS at lysine 7 can dramatically affect its aggregation. Therefore, lysine 7 of MAVS may be an important site for determining MAVS function, even though it does not localize to the CARD. Indeed, other modifications at lysine 7 of MAVS that affect MAVS function have been previously identified (15, 34, 50–52). Structural modeling indicates that, compared to succinylation of MAVS at lysine 7, acetylation of MAVS at lysine 7 can increase the distance between MAVS and the components of the MAVS/RIG-I complex, leading to attenuation of MAVS-RIG-I complex formation and subsequent RLR signaling activation, further highlighting that the lysine 7 of MAVS is a critical residue for controlling MAVS function.

Notably, other residues of MAVS besides lysine 7 have been reported to be modified by various PTMs (19). TRIM25 or MARCH5 catalyzes K48-linked ubiquitination at K7, leading to the destabilization of MAVS or reduction of MAVS aggregates (15, 34). Succinylation at K7 activates MAVS, while desuccinylation at K7 by SIRT5 suppresses MAVS-mediated RLR signaling. Acetylation at K7 inhibits MAVS, but deacetylation at K7 by SIRT3 augments MAVS-mediated RLR signaling. When K7 of MAVS is mutated to arginine, the ubiquitination, succinylation, acetylation, and some other unspecified modifications at K7 are simultaneously blocked. It remains unclear to what extent deacetylation/desuccinylation of MAVS at lysine 7 contributes to the regulation of MAVS function in the RLR signaling, as determined by the use of the K7R mutant. Further investigation of this question may open a window for understanding the physiological function of MAVS deacetylation/desuccinylation in type I interferon signaling.

While the in vitro data obtained in this study support a role for SIRT3 in the regulation of MAVS-dependent immunity, the in vivo data based on *Sirt3* knockout mice do not prove that SIRT3 acts exclusively through MAVS. In the future, obtaining *Sirt3*/*Mavs* double knockout mice will allow us to define MAVS-dependent and independent effects of SIRT3 in antiviral immunity.

Materials and Methods

The following is a brief description of *Materials and Methods*, and the description of *Materials and Methods* in detail in *SI Appendix*.

Mice. Six- to eight-week-old mice were used in the experiments. Same-sex (male) littermates were randomly assigned to the experimental groups. All analyses were blinded.

Zebrafish. CRISPR/Cas9 was used to generate *sirt3* knockout zebrafish. *Sirt3* sgRNA was designed using an online CRISPR design tool (http://crispor.gi.ucsc.edu/crispor.py).

Cell Culture. Primary MEFs were prepared from embryos at 12.5 to 14.5 embryonic days. Bone marrow cells were isolated from the mouse femur.

Luciferase Reporter Assays. Luciferase activity was determined using the dual-luciferase reporter assay system (Promega) at 18 to 24 h posttransfection.

Quantitative Real-Time PCR (qPCR). MonAmp™ SYBR® Green qPCR Mix (high Rox) was used for qPCR assays. Primers for qPCR are listed in *SI Appendix*, Table S2.

CRISPR-Cas9 Knockout Cell Lines. sgRNA sequence was ligated into LentiCRISPRv2 plasmid and then cotransfected with viral packaging plasmids (psPAX2 and pMD2G) into HEK293T cells.

Immunoblotting and IP Assay. Cell lysates were separated by SDS-PAGE, transferred onto a polyvinylidene difluoride membrane, blocked with 5% (w/v) nonfat milk, probed with the indicated primary antibodies and corresponding secondary antibodies.

Immunofluorescence Confocal Microscopy. Cells were stained with the indicated primary antibodies followed by incubation with fluorescent dye-conjugated secondary antibodies.

Proximity Ligation Assay (PLA). PLA was performed according to the manufacturer's instructions for the Duolink In Situ Red Starter Kit Mouse/Rabbit.

Generation of Anti-Ac-K7-MAVS Antibody. A MAVS K7 site-specific acetylation antibody (anti-Ac-K7-MAVS) was generated by using a human MAVS acetylated peptide [MPFAED(ac-K)TYKYIC] as an antigen.

Semidenaturing Detergent Agarose Gel Electrophoresis (SDD-AGE) Assay. Crude mitochondrial and cytosolic extracts were prepared from HEK293T or MEF cells by differential centrifugation.

Flow Cytometry Assays for VSV-GFP Infected Cells. Cells were infected with VSV-GFP virus (MOI = 0.1) for the indicated time, then harvested and washed with PBS. Cells were counted at 10,000 cells, and subsequent analyses were performed on Beckman CytoFLEXS.

Cell Apoptosis Analysis. FITC Annexin V Apoptosis Detection Kit I (BD Pharmingen) was used to measure the effect of 3-TYP (10 to 200 μM) on cell apoptosis of THP-1 cells.

Lentivirus-Mediated Gene Transfer. Cells were transfected with pHAGE-SIRT3, pHAGE-SIRT3-H248Y, pHAGE-Sirt3, or the empty vector together with the packaging vectors pSPAX2 and pMD2G.

Structure Modeling. We used PyMOL (http://www.pymol.org) to obtain the structure model of K7 acetylation and succinylation.

Virus Infection in Mice. Age- and sex-matched (male) $Sirt3^{+/+}$ and $Sirt3^{-/-}$ mice were infected with VSV. For viral infection in $Sirt^{+/+}Sirt5^{+/+}$ and $Sirt3^{-/-}Sirt5^{-/-}$ mice, age- and sex-matched (male) mice were injected intraperitoneally with VSV or EMCV.

Viral Infection in Zebrafish. Zebrafish larvae (3 dpf) were placed in a disposable 60-mm cell culture dish filled with 3 mL egg water and 2 mL SVCV (~2.0×10^8 $TCID_{50}$/mL) culture medium, or 4.7 mL egg water and 0.3 mL GCRV-II.

Statistical Analysis. GraphPad Prism 8.0 software (GraphPad Software, San Diego, CA) was used for all statistical analyses.

Data, Materials, and Software Availability. All study data are included in the article and/or *SI Appendix*.

ACKNOWLEDGMENTS. We thank Drs. Hongbing Shu, Bo Zhong, Mingzhou Chen, Chunfu Zheng, Yaping Wang, and Hong Tang for providing reagents. We thank Yan Wang and Fang Zhou at the Core Facility of Institute of Hydrobiology for flow cytometry and confocal microscopy. This work was supported by the Strategic Priority Research Program of the Chinese Academy of Sciences [XDB0730300 and XDA24010308]; National Natural Science Foundation of China [32273171]; the National Key Research and Development Program of China [2022YFF1000302 and 2018YFD0900602]; the Natural Science Foundation of Hubei Province of China [2022CFA110], and "Agricultural Biological Breeding-2030" major project [2023ZD04065].

Author affiliations: [a]Key Laboratory of Breeding Biotechnology and Sustainable Aquaculture, Institute of Hydrobiology, Chinese Academy of Sciences, Wuhan 430072, China; [b]Hubei Hongshan Laboratory, Wuhan 430070, China; [c]The Innovation of Seed Design, Chinese Academy of Sciences, Wuhan 430072, China; [d]University of Chinese Academy of Sciences, Beijing 100049, China; and [e]The Key laboratory of Aquaculture Disease Control, Ministry of Agriculture, Wuhan 430072, China

1. E. Meylan *et al.*, Cardif is an adaptor protein in the RIG-I antiviral pathway and is targeted by hepatitis C virus. *Nature* **437**, 1167–1172 (2005).
2. R. B. Seth, L. Sun, C. K. Ea, Z. J. Chen, Identification and characterization of MAVS, a mitochondrial antiviral signaling protein that activates NF-kappaB and IRF 3. *Cell* **122**, 669–682 (2005).
3. L. G. Xu *et al.*, VISA is an adapter protein required for virus-triggered IFN-beta signaling. *Mol. Cell* **19**, 727–740 (2005).
4. T. Kawai *et al.*, IPS-1, an adaptor triggering RIG-I- and Mda5-mediated type I interferon induction. *Nat. Immunol.* **6**, 981–988 (2005).
5. H. Ishikawa, G. N. Barber, STING is an endoplasmic reticulum adaptor that facilitates innate immune signalling. *Nature* **455**, 674–678 (2008).
6. S. Liu *et al.*, Phosphorylation of innate immune adaptor proteins MAVS, STING, and TRIF induces IRF3 activation. *Science* **347**, aaa2630 (2015).
7. J. Rehwinkel, M. U. Gack, RIG-I-like receptors: Their regulation and roles in RNA sensing. *Nat. Rev. Immunol.* **20**, 537–551 (2020).
8. X. Tan, L. Sun, J. Chen, Z. J. Chen, Detection of microbial infections through innate immune sensing of nucleic acids. *Annu. Rev. Microbiol.* **72**, 447–478 (2018).
9. W. Zhang *et al.*, Lactate is a natural suppressor of RLR signaling by targeting MAVS. *Cell* **178**, 176–189.e15 (2019).
10. D. Liu, V. M. Johnson, H. B. Pakrasi, A reversibly induced CRISPRi system targeting Photosystem II in the cyanobacterium Synechocystis sp. PCC 6803. *ACS Synth. Biol.*, 1441–1449 (2020).
11. T. Li *et al.*, O-GlcNAc transferase links glucose metabolism to MAVS-mediated antiviral innate immunity. *Cell Host Microbe* **24**, 791–803.e6 (2018).
12. W. Zhu *et al.*, TRAF3IP3 mediates the recruitment of TRAF3 to MAVS for antiviral innate immunity. *EMBO J.* **38**, e102075 (2019).
13. S. Z. Li *et al.*, Phosphorylation of MAVS/VISA by Nemo-like kinase (NLK) for degradation regulates the antiviral innate immune response. *Nat. Commun.* **10**, 3233 (2019).
14. N. Song *et al.*, MAVS O-GlcNAcylation is essential for host antiviral immunity against lethal RNA viruses. *Cell Rep.* **28**, 2386–2396.e5 (2019).
15. Y. S. Yoo *et al.*, The mitochondrial ubiquitin ligase MARCH5 resolves MAVS aggregates during antiviral signalling. *Nat. Commun.* **6**, 7910 (2015).
16. S. Yang *et al.*, Control of antiviral innate immune response by protein geranylgeranylation. *Sci. Adv.* **5**, eaav7999 (2019).
17. T. Dai *et al.*, FAF1 regulates antiviral immunity by inhibiting MAVS but is antagonized by phosphorylation upon viral infection. *Cell Host Microbe* **24**, 776–790.e5 (2018).
18. Z. Zhang *et al.*, Acetylation-dependent deubiquitinase OTUD3 controls MAVS activation in innate antiviral immunity. *Mol. Cell* **79**, 304–319.e7 (2020).
19. B. Liu, C. Gao, Regulation of MAVS activation through post-translational modifications. *Curr. Opin. Immunol.* **50**, 75–81 (2018).
20. Y. L. Deribe, T. Pawson, I. Dikic, Post-translational modifications in signal integration. *Nat. Struct. Mol. Biol.* **17**, 666–672 (2010).
21. J. Zhu *et al.*, Arginine monomethylation by PRMT7 controls MAVS-mediated antiviral innate immunity. *Mol. Cell* **81**, 3171–3186.e8 (2021).
22. X. Liu *et al.*, SIRT5 impairs aggregation and activation of the signaling adaptor MAVS through catalyzing lysine desuccinylation. *EMBO J.* **39**, e103285 (2020).
23. T. Finkel, C. X. Deng, R. Mostoslavsky, Recent progress in the biology and physiology of sirtuins. *Nature* **460**, 587–591 (2009).
24. E. Verdin, M. D. Hirschey, L. W. Finley, M. C. Haigis, Sirtuin regulation of mitochondria: Energy production, apoptosis, and signaling. *Trends Biochem. Sci.* **35**, 669–675 (2010).
25. K. A. Anderson, M. F. Green, F. K. Huynh, G. R. Wagner, M. D. Hirschey, SnapShot: Mammalian sirtuins. *Cell* **159**, 956–956.e1 (2014).
26. J. Zhang *et al.*, Mitochondrial sirtuin 3: New emerging biological function and therapeutic target. *Theranostics* **10**, 8315–8342 (2020).
27. C. Guan *et al.*, SIRT3-mediated deacetylation of NLRC4 promotes inflammasome activation. *Theranostics* **11**, 3981–3995 (2021).
28. X. Sheng, I. M. Cristea, The antiviral sirtuin 3 bridges protein acetylation to mitochondrial integrity and metabolism during human cytomegalovirus infection. *PLoS Pathog.* **17**, e1009506 (2021).
29. J. Hou *et al.*, USP18 positively regulates innate antiviral immunity by promoting K63-linked polyubiquitination of MAVS. *Nat. Commun.* **12**, 2970 (2021).
30. M. D. Hirschey *et al.*, SIRT3 regulates mitochondrial fatty-acid oxidation by reversible enzyme deacetylation. *Nature* **464**, 121–125 (2010).
31. U. Galli *et al.*, Identification of a sirtuin 3 inhibitor that displays selectivity over sirtuin 1 and 2. *Eur. J. Med. Chem.* **55**, 58–66 (2012).
32. E. Ciarlo *et al.*, Sirtuin 3 deficiency does not alter host defenses against bacterial and fungal infections. *Sci. Rep.* **7**, 3853 (2017).
33. H. Inuzuka *et al.*, Acetylation-dependent regulation of Skp2 function. *Cell* **150**, 179–193 (2012).
34. C. Castanier *et al.*, MAVS ubiquitination by the E3 ligase TRIM25 and degradation by the proteasome is involved in type I interferon production after activation of the antiviral RIG-I-like receptors. *BMC Biol.* **10**, 44 (2012).
35. M. Yoneyama, T. Fujita, Structural mechanism of RNA recognition by the RIG-I-like receptors. *Immunity* **29**, 178–181 (2008).
36. X. Cai *et al.*, Opposing effects of deubiquitinase OTUD3 in innate immunity against RNA and DNA viruses. *Cell Rep.* **39**, 110920 (2022).
37. U. Ashraf *et al.*, Spring viraemia of carp virus: Recent advances. *J. Gen. Virol.* **97**, 1037–1051 (2016).
38. Y. Rao, J. Su, Insights into the antiviral immunity against grass carp (Ctenopharyngodon idella) reovirus (GCRV) in grass carp. *J. Immunol. Res.* **2015**, 670437 (2015).
39. T. Heinonen, E. Ciarlo, D. Le Roy, T. Roger, Impact of the dual deletion of the mitochondrial sirtuins SIRT3 and SIRT5 on anti-microbial host defenses. *Front. Immunol.* **10**, 2341 (2019).
40. B. Wu *et al.*, Molecular imprinting as a signal-activation mechanism of the viral RNA sensor RIG-I. *Mol. Cell* **55**, 511–523 (2014).
41. P. Onyango, I. Celic, J. M. McCaffery, J. D. Boeke, A. P. Feinberg, SIRT3, a human SIR2 homologue, is an NAD-dependent deacetylase localized to mitochondria. *Proc. Natl. Acad. Sci. U.S.A.* **99**, 13653–13658 (2002).
42. T. Shi, F. Wang, E. Stieren, Q. Tong, SIRT3, a mitochondrial sirtuin deacetylase, regulates mitochondrial function and thermogenesis in brown adipocytes. *J. Biol. Chem.* **280**, 13560–13567 (2005).
43. B. Schwer, J. Bunkenborg, R. O. Verdin, J. S. Andersen, E. Verdin, Reversible lysine acetylation controls the activity of the mitochondrial enzyme acetyl-CoA synthetase 2. *Proc. Natl. Acad. Sci. U.S.A.* **103**, 10224–10229 (2006).
44. F. Hou *et al.*, MAVS forms functional prion-like aggregates to activate and propagate antiviral innate immune response. *Cell* **146**, 448–461 (2011).
45. Y. Nishida *et al.*, SIRT5 regulates both cytosolic and mitochondrial protein malonylation with glycolysis as a major target. *Mol. Cell* **59**, 321–332 (2015).
46. M. J. Rardin *et al.*, SIRT5 regulates the mitochondrial lysine succinylome and metabolic networks. *Cell Metab.* **18**, 920–933 (2013).
47. M. Walter *et al.*, SIRT5 is a proviral factor that interacts with SARS-CoV-2 Nsp14 protein. *PLoS Pathog.* **18**, e1010811 (2022).
48. H. Xu *et al.*, Structural basis for the prion-like MAVS filaments in antiviral innate immunity. *Elife* **3**, e01489 (2014).
49. X. Cai *et al.*, Prion-like polymerization underlies signal transduction in antiviral immune defense and inflammasome activation. *Cell* **156**, 1207–1222 (2014).
50. Y. J. Park *et al.*, Dual targeting of RIG-I and MAVS by MARCH5 mitochondria ubiquitin ligase in innate immunity. *Cell Signal.* **67**, 109520 (2020).
51. S. Jin *et al.*, Tetherin suppresses type I interferon signaling by targeting MAVS for NDP52-mediated selective autophagic degradation in human cells. *Mol. Cell* **68**, 308–322.e4 (2017).
52. S. Jin, J. Cui, BST2 inhibits type I IFN (interferon) signaling by accelerating MAVS degradation through CALCOCO2-directed autophagy. *Autophagy* **14**, 171–172 (2018).